Highlights

Cognitive Warfare, Hybrid Pressure, and Sovereign Resilience: An Operations Research Framework Applied to the Iranian Case (2017–2026)

Rahimeh Neamatian Monemi, Shahin Gelareh, Nelson Maculan

- Proves existence and local stability of a defender-MDP coupled equilibrium.
- Formal theorem distinguishes it from autonomous-ODE Lyapunov stability.
- Attacker self-limitation is derived from Bellman optimality, not assumed.
- Validated via 30 randomised network instances and full value iteration.
- Iran's 2017–2026 case sits 25x above the computed collapse boundary.

arXiv:2607.01894v1 [math.OC] 2 Jul 2026

Cognitive Warfare, Hybrid Pressure, and Sovereign Resilience: An Operations Research Framework Applied to the Iranian Case (2017–2026)

Rahimeh Neamatian Monemi[a], Shahin Gelareh[b,*], Nelson Maculan[c]

[a]*Sharkey Predictim Globe*
[b]*Département R&T, IUT de Béthune, Université d'Artois, F-62000, Béthune, France*
[c]*Federal University of Rio de Janeiro, COPPE-PESC, P.O. Box 68511, Rio de Janeiro, RJ 21941-972, Brazil*

Abstract

A defending state facing sustained economic, media, and psychological pressure from an adversary that continuously re-optimises its campaign poses a problem that existing attacker-defender models in operations research do not directly resolve, because they treat the defender's state as a discrete allocation rather than a continuous, slow-moving institutional process. We formulate a coupled dynamical system in which grievance and institutional resilience evolve continuously while pressure intensity is chosen by an optimising Markov decision process, prove existence and local stability of the resulting equilibrium, and prove a formal result distinguishing it from standard feedback-stability analysis and from a stationary Markov chain treated in isolation. We validate the framework computationally using thirty randomised network instances, full value iteration, and a documented case study of cognitive warfare directed at Iran (2017–2026). The historically calibrated case sits approximately twenty-five times above the computed operational collapse boundary, and a greedy seeding policy reaches eighty-seven percent average network penetration across the randomised instances, significantly above a degree-centrality baseline. A practitioner can use the equilibrium and boundary computation to assess where a specific case sits relative to collapse, rather than relying on an unverified comparison between opposing pressure intensities.

Keywords: Cognitive warfare, Influence maximisation, Markov decision processes, Sovereign resilience

1. Introduction

Between 2017 and 2026, Iran's currency lost over 97 per cent of its value against the dollar and the poverty headcount rose by eight percentage points under the weight of economic sanctions (Wikipedia, 2026f; World Bank, 2023), while a parallel satellite-television and social-media campaign targeting the Iranian population was documented at an estimated potential reach of up to 80 per cent of internet users (Internet Society, 2024; DataReportal, 2022). The question this paper addresses is not whether those instruments were deployed at scale — they were — but whether, and under what formal conditions, a target state's institutional consolidation mechanism can render them self-defeating regardless of their intensity. Cognitive warfare, broadly defined as the deliberate use of information, economic pressure, and psychological operations to alter how target populations form beliefs and make decisions (du Cluzel, F., 2021; Claverie, B., du Cluzel, F., 2021), has been theorised as the *sixth domain* of warfare in NATO documents after 2020 (Deppe and Schaal, 2024; Anonymous, 2026).

A distinguishing feature of cognitive warfare is its integration with *psychological operations* (PSYOP) — structured programmes designed to influence the emotions, motives, objective reasoning, and behaviour of target audiences (Claverie, B., du Cluzel, F., 2021). Where classical PSYOP relied on leaflets, radio broadcasts, and face-to-face influence, modern cognitive warfare exploits algorithmically curated social media feeds, satellite television, and computational propaganda to achieve influence at population scale (Deppe and Schaal, 2024).

From an OR perspective, cognitive warfare constitutes a class of *adversarial decision problems* over networked social systems, combining: influence maximisation (Kempe, D., Kleinberg, J., Tardos, É., 2003), bilevel Stackelberg programming (Dempe, S., 2002), stochastic network interdiction (Cormican, K.J., Morton, D.P., Wood, R.K., 1998), and system dynamics (Sterman, J.D., 2000).

*Corresponding author
Email address: shahin.gelareh@gmail.com (Shahin Gelareh)

Existing OR treatments of attacker-defender interaction do not resolve this problem directly. Stochastic network interdiction (Cormican, K.J., Morton, D.P., Wood, R.K., 1998) and Stackelberg security games (Dempe, S., 2002) optimise a *single-shot* or *repeated-but-stationary* defensive allocation against a fixed threat model; the most recent systematic review of this literature (Hunt and Zhuang, 2024) catalogues 127 attacker-defender formulations without one that couples a continuous, sanctions-driven grievance process to an MDP-optimising adversary whose policy itself responds to that process. System dynamics (Sterman, J.D., 2000) and influence-maximisation (Kempe, D., Kleinberg, J., Tardos, É., 2003) models, taken separately, each capture one half of the mechanism — the slow feedback structure or the fast network propagation — but neither, on its own, can represent an adversary that observes the discretised social-stability state and *re-optimises* cognitive pressure in response, which is precisely the channel through which the self-limiting dynamic documented below arises. This gap, not merely the empirical novelty of the Iranian case, motivates the coupled formulation developed in Section 4.

This paper applies these tools to the Iranian case, spanning 2017 to 2026. The timeline encompasses the launch of Iran International Television (2017), the intensification of economic sanctions (2018–2022), the social mobilisation following the death of Mahsa Amini (2022), and the kinetic conflict initiated on 28 February 2026 (House of Commons Library, 2026a). Iran's continued institutional functioning, leadership transition, and negotiated ceasefire provide the analytical terminus.

One may ask whether the proposed Adversarial Resilience Equilibrium is merely Lyapunov asymptotic stability of a feedback ODE applied in a new substantive context. If the adversary's pressure level is treated as an exogenous constant and one asks only whether the grievance equilibrium is a stable fixed point, the resulting condition is structurally identical to a textbook Lyapunov-stability criterion for a logistic-versus-saturating feedback system, and Theorem 1 makes no claim of departing from that classical result. The distinction lies in what ARE adds: it requires the adversary's intensity to be chosen by an optimising Markov decision process that observes the social-stability state and re-optimises in each period, coupling the grievance dynamics to a closed-loop adversarial layer (Section 3.4). Theorem 2 formalises this difference by constructing a specific prediction that the autonomous-ODE formalism cannot generate: that the attacker's optimal intensity is lower at the highest mobilisation state than at intermediate ones, because reaching full escalation turns negative for the attacker under optimal play. This prediction is verified computationally in Section 6.2. Removing the MDP coupling collapses the model's prediction from "the attacker self-limits because pressing further is suboptimal" to "the grievance variable happens to be stable" — a materially weaker and less falsifiable claim.

Three questions guide the paper and are each answered in Sections 6–8: whether coupling a continuous grievance-resilience system to an optimising MDP adversary admits a formally provable equilibrium distinct from classical autonomous-ODE stability; whether that coupling generates a computationally verifiable self-limitation mechanism rather than an assumed one; and how far the historically calibrated Iranian case sits from the resulting collapse boundary, and which factors govern that margin.

The central contribution is a formally proved Adversarial Resilience Equilibrium for a grievance-resilience dynamical system coupled to an optimising MDP adversary, together with a Non-Equivalence Theorem (Theorem 2) showing the result is not reducible to autonomous-ODE Lyapunov stability or to stationary-distribution analysis of an uncoupled Markov chain. Two supporting results accompany it: a computationally verified self-limitation mechanism (Proposition 2), derived from the reward structure rather than assumed; and a reproducible computational study — randomised multi-instance influence-maximisation with baseline comparison and significance testing, value iteration over a fully specified transition model, and a Shapley-style instrument decomposition — applied to the Iranian case (2017–2026) with all reported figures generated by the companion script rather than set by hand. Numerical calibration to published battlefield and economic data (Section 6) is supporting evidence for these contributions, not a standalone claim.

Remark 1 (Epistemological note)**.** *This article analyses the structural logic of cognitive warfare operations from a neutral OR standpoint. All actors are treated as rational strategic agents. No normative judgement is made regarding the legitimacy, legality, or ethics of any actor's conduct. All figures are sourced to verifiable publications or derived mathematically, as indicated.*

The article is organised as follows. Section 2 surveys the four relevant OR methodology streams. Section 3 establishes the mathematical framework. Section 4 presents the Adversarial Resilience Equilibrium and its formal results. Section 5 applies the framework to the Iranian case (2017–2026) across four documented phases. Section 6 reports the numerical experiments and factor dominance analysis. Section 7 discusses results, implications, limitations, and future work. Section 8 concludes.

2. Literature Review and Research Gap Analysis

Operations Research literature reviews are organised by methodology stream, not by application domain. This section covers four streams: exact and game-theoretic attacker-defender formulations, network interdiction and influence maximisation, stochastic control via Markov decision processes, and system dynamics. An application-domain survey of cognitive-warfare studies alone would not constitute an OR literature review; that material is instead woven into the calibration discussion of Section 5.2.

2.1. Exact and Game-Theoretic Attacker-Defender Formulations

Bilevel and Stackelberg security games are the natural OR formalism for an attacker choosing pressure instruments against a strategically responding defender (Dempe, S., 2002). Hunt and Zhuang (2024) systematically review 127 attacker-defender formulations published over fifteen years and find that the overwhelming majority either solve a single-shot resource-allocation problem or assume a stationary threat model; very few couple the defender's state to a continuous process that the attacker observes and responds to dynamically. Bustamante-Faúndez et al. (2024) make recent, substantial progress on the computational side, proposing compact formulations for a broad class of Stackelberg security games and reporting an extensive computational study — a methodological strength this manuscript does not attempt to match, since the present contribution is the coupling structure, not solver performance. What neither of these strong, recent contributions provides is a defender whose response is itself a continuous, path-dependent state variable (the grievance-resilience pair (G, ρ) of Section 4) rather than a discrete protection allocation; this is the specific gap the ARE construction addresses.

2.2. Network Interdiction and Influence Maximisation

Stochastic network interdiction (Cormican, K.J., Morton, D.P., Wood, R.K., 1998) and its modern risk-averse and distributionally robust extensions (Sadana and Delage, 2023; Vaziri et al., 2025) formalise the defender's budget-constrained edge-removal problem central to Section 6.1 (equation (16)). Sadana and Delage (2023) show that randomised interdiction strategies can strictly dominate deterministic ones under distributional ambiguity — a result this manuscript does not exploit (the interdiction budget in Section 6.1 is deterministic), flagged here as a concrete avenue for tightening the influence-maximisation experiment in future work. Influence maximisation on social networks (Kempe, D., Kleinberg, J., Tardos, É., 2003) supplies the submodular greedy guarantee used directly in Algorithm 1; this manuscript's contribution at this layer is the randomised multi-instance validation protocol with baseline comparison (Table 6), not a new approximation result.

2.3. Stochastic Control via Markov Decision Processes

The Bellman equation (Bellman, 1957) underlies Section 3.4 directly; this manuscript's contribution is the explicit overshoot-penalty reward construction (equation (21)) that makes the self-limitation result of Proposition 2 a derived consequence of Bellman optimality rather than an assumed narrative. The MDP literature on adversarial and security policy applications is large; within the scope verified for this manuscript, the closest methodological relatives are the attacker-defender formulations of §2.1, which solve for a static allocation rather than a state-contingent intensity policy.

2.4. System Dynamics and Nonlinear Feedback Stability

System dynamics (Sterman, J.D., 2000) provides the causal-loop formalism of Table 4 and the reinforcing/balancing loop vocabulary used throughout. Anderson et al. (2023) argue, in a recent agenda-setting piece for the operations-management community, that system dynamics is under-exploited for public-policy problems with feedback, delay, and multiple stakeholders precisely because such models are rarely coupled to an optimising decision layer — the gap this manuscript's MDP coupling (Section 4) is designed to close for the specific case of an optimising adversary.

2.5. Where the Field Was Heading, and What Blocked It

The attacker-defender literature of §2.1 was converging, over the period covered by Hunt and Zhuang (2024)'s review, toward increasingly realistic resource-allocation models — multi-period, robust, and behaviourally boundedly-rational variants all appear in their taxonomy. What that convergence did not produce is a formulation in which the defender's state is a *continuous, slow-moving institutional variable* rather than a discrete allocation choice, because doing so requires coupling two normally separate OR sub-fields (MDP-based stochastic control and system-dynamics feedback modelling) that are rarely combined in the same paper. This is the specific barrier Theorem 2 and the reduced-form construction of

§4.1 are built to remove; doing so opens a direction the existing literature does not yet pursue: applying the same coupling to other slow-institutional-variable security problems (border stability, critical-infrastructure trust erosion, alliance cohesion) where a defender's "state" is similarly a continuous, path-dependent quantity rather than a discrete posture.

Table 1: Contribution positioning relative to representative recent OR literature

Property	Hunt and Zhuang (2024)	Bustamante-Faúndez et al. (2024)	Sadana and Delage (2023)	Sterman, J.D. (2000)	**This paper**
Defender state is continuous, not a discrete allocation	No	No	No	Yes (uncoupled)	Yes
Adversary policy is MDP-optimised and state-contingent	Partial	Partial	No	No	Yes
Formal non-equivalence to autonomous-ODE stability proved	N/A	N/A	N/A	N/A	Proved
Self-limitation derived from reward structure (not assumed)	No	No	No	No	Proved
Randomised multi-instance computational validation with baselines	Varies	Yes	Yes	No	Yes

The research gap that follows from Table 1 is narrow and specific: no reviewed formulation couples a continuous, system-dynamics state to an MDP-optimising adversary with a formally distinguished equilibrium concept. Section 4 addresses exactly this gap.

3. Mathematical Framework

3.1. Bilevel Optimisation Formulation

Let the cognitive warfare system be modelled as a two-level Stackelberg game. The attacker selects $\mathbf{x} \in \mathcal{X} \subseteq \mathbb{R}^m$ (cognitive instruments) to maximise strategic objective $f(\mathbf{x}, \mathbf{y})$. The defender selects $\mathbf{y} \in \mathcal{Y} \subseteq \mathbb{R}^n$ to minimise social destabilisation:

$$\min_{\mathbf{y} \in \mathcal{Y}} g(\mathbf{x}, \mathbf{y}). \tag{1}$$

The full bilevel problem is:

$$\max_{\mathbf{x} \in \mathcal{X}} \; f(\mathbf{x}, \mathbf{y}^*(\mathbf{x})) \quad \text{s.t.} \quad \mathbf{y}^*(\mathbf{x}) \in \arg\min_{\mathbf{y} \in \mathcal{Y}} g(\mathbf{x}, \mathbf{y}). \tag{2}$$

Problem (2) is NP-hard in general (Dempe, S., 2002). In the Iranian context, $\mathcal{X}$ includes sanctions intensity, media penetration, psychological operation budgets, and social media narrative injection intensity. The defender's set $\mathcal{Y}$ includes capital controls, internet interdiction budget, security force deployment, and ideological consolidation investment.

3.2. Psychological Operations Layer

Classical psychological operations theory (Pratkanis, 2007) models attitude change as a function of message credibility $c \in [0, 1]$, repetition $r \geq 0$, and audience susceptibility $\theta \in [0, 1]$. The *belief shift* Δb in a target audience is approximated by:

$$\Delta b = \theta \cdot c \cdot \left(1 - e^{-\lambda r}\right), \quad \lambda > 0, \tag{3}$$

where λ is the saturation rate of repetition exposure. This equation captures: (i) the diminishing marginal returns to message repetition ($\partial^2 \Delta b / \partial r^2 < 0$); (ii) the multiplicative role of credibility ($c = 0$ implies $\Delta b = 0$ regardless of repetition); and (iii) the population-level heterogeneity through θ.

In the Iranian cognitive warfare context, the satellite television channel functions as a high-credibility ($c \approx 0.7$, inferred from audience retention data), high-repetition (r proportional to daily broadcast hours) instrument directed at a susceptible diaspora and VPN-connected domestic audience. Integration with influence maximisation (Section 3.3) yields a *cognitive-psychological cascade*: the PSYOP model governs individual belief shift at the node level, while the Independent Cascade Model (Kempe, D., Kleinberg, J., Tardos, É., 2003) propagates these shifts through the social network.

Formally, let belief shift at seed node u be Δb_u as per equation (3). The edge activation probability in the Independent Cascade Model is then set as:

$$p(u, v) = \min(1,\ \alpha \cdot \Delta b_u \cdot \omega_{uv}), \tag{4}$$

where $\alpha > 0$ is a scaling constant and $\omega_{uv} \in (0, 1]$ is the social tie strength between u and v. This coupling links the PSYOP layer directly to the graph-theoretic influence model.

3.3. Influence Maximisation on the Social Network

Let $\mathcal{G} = (V, E, p)$ be the Iranian social information network. The influence maximisation problem seeks $S \subseteq V$, $|S| = k$, maximising:

$$\sigma(S) = \mathbb{E}[|A_T(S)|], \tag{5}$$

where $A_T(S)$ is the set of eventually activated nodes under the Independent Cascade Model (Kempe, D., Kleinberg, J., Tardos, É., 2003). Since $\sigma(\cdot)$ is monotone and submodular, the greedy algorithm achieves the approximation ratio $(1 - 1/e) \approx 0.632$ (Kempe, D., Kleinberg, J., Tardos, É., 2003):

$$\sigma(S_{\text{greedy}}) \ \geq\ \left(1 - \tfrac{1}{e}\right) \sigma(S^*). \tag{6}$$

3.4. Markov Decision Process Model

Societal stability evolves as MDP $\mathcal{M} = (S, A, P, R, \gamma)$ with $S = \{s_1, \ldots, s_5\}$ (five stability states from full stability to open high-intensity mobilisation), discount factor $\gamma = 0.95$, and the Bellman equation:

$$V^*(s) = \max_{a \in A} \left[R(s, a) + \gamma \sum_{s' \in S} P(s'|s, a) V^*(s') \right]. \tag{7}$$

3.5. Econometric Sanctions Model

Laudati and Pesaran (2023) establish that Iran's average annual growth penalty from sanctions is 1–2 percentage points, with the World Bank (2023) confirming a per-capita GDP contraction of -0.6% p.a. between 2011 and 2020. Sanctions impose budget constraint:

$$\sum_j p_j c_j \leq w - \delta(\mathbf{x}_s), \quad \delta(\mathbf{x}_s) \geq 0, \tag{8}$$

where $\delta(\mathbf{x}_s)$ is increasing in sanctions intensity. Farzanegan and Habibi (2025) document the Gini coefficient rising from 34.0 (2011) to 37.4 (2018), consistent with the differential impact of δ on middle-income households. Specifically, Farzanegan and Habibi (2025) find that by 2019 Iran's middle class was 28% smaller than its synthetic counterfactual, with sanctions causing an average annual per-capita income loss of approximately \$3,000 between 2012 and 2019. Using a structural vector-autoregression on quarterly conflict-event data, Farzanegan and Gutmann (2024) report a result directly relevant to the self-limitation mechanism of Proposition 2: an unexpected increase in sanction intensity raises civil-disorder and terrorism risk in Iran but *lowers* the risk of escalation to civil war. This is independent econometric evidence, external to the bilevel and MDP framework developed here, that higher adversarial pressure does not translate monotonically into higher destabilisation risk at the most severe end of the outcome scale — the same qualitative pattern this paper derives from Bellman optimality rather than from a reduced-form regression, for a different mechanism (an optimising attacker's policy reversal rather than a population-level conflict-risk regression), but a structurally analogous finding that we flag as independent corroboration rather than as evidence for the formal mechanism itself.

4. Adversarial Resilience Equilibrium

This section states the assumptions, the reduced-form dynamics, and the formal results on which the Adversarial Resilience Equilibrium (ARE) rests.

4.1. Reduced-Form Dynamics and Assumptions

The six-variable causal loop system of Table 4 is intractable in closed form. We work instead with a scalar reduction for the grievance index $G(t) \in [0, 1]$, in which the reinforcing channel (Loop R1: sanctions, currency depreciation, and external-media amplification) is represented as logistic self-amplification, and the balancing channel (Loop B2: institutional consolidation) is represented by the Hill-type mobilisation function already defined in equation (14):

$$\frac{dG}{dt} = g_{R1}\,\alpha(t)\,G\,(1-G) \;-\; g_{B2}\,\pi_m(G) \;+\; \epsilon(t), \tag{9}$$

where $\alpha(t) \in \{\alpha_0, \alpha_1\}$ is the piecewise-constant PSYOP amplification level of Section 3.2 and $\epsilon(t)$ is a sparse exogenous shock term (the Amini event). A coupled resilience variable $\rho(t) \in [0, 1]$ evolves on a slower timescale,

$$\frac{d\rho}{dt} = g_{B2}\,\pi_m(G)\,(1-\rho) \;-\; \kappa\,G\,\rho \;+\; \gamma\,\mathbb{1}[\text{kinetic regime}]\,(1-\rho), \tag{10}$$

where $\kappa > 0$ is the institutional-erosion rate and $\gamma > 0$ is the rally-effect gain activated only during the kinetic-escalation window (Levy, J.S., 1989). The notation $R(G)$ for institutional response is avoided here because it collides with both the MDP reward $R(s, a)$ of Section 3.4 and the network-reliability function $R(\mathcal{G}, k)$ used in Section 4, and would leave the institutional-response channel without an explicit law of motion. Folding it into $\pi_m(G)$ avoids this ambiguity while preserving the qualitative loop structure of Table 4: resilience rises with the consolidation response (itself proportional to mobilisation pressure) and erodes with raw grievance.

Table 2: Assumption traceability matrix for the reduced-form dynamics

ID	Statement and rationale	Depends on	Status
A1	Quasi-static reduction: the five auxiliary causal-loop variables (currency, inflation, poverty, mobilisation response, consolidation) adjust fast relative to G and ρ, justifying the two-state reduction (9)–(10).	Thm. 1, Prop. 2	Essential
A2	$\pi_m(\cdot)$ is C^1 on $[0, 1]$, strictly increasing, $\pi_m(0) = 0$, $\pi'_m(0) = 0$ for $\alpha_H > 1$ (Hill saturation).	Thm. 1	Essential
A3	$\alpha(t)$ is piecewise constant on $\{\alpha_0, \alpha_1\}$, bounded and strictly positive.	Thm. 1, Prop. 2	Technical
A4	$\epsilon(t)$ is supported on a measure-zero/short-duration shock set; baseline existence/stability analysis sets $\epsilon \equiv 0$ and treats shocks as instantaneous state jumps.	Thm. 1	Convenience (relaxed in §6.4)
A5	κ, γ in equation (10) are constants fitted to reproduce the qualitative timeline of Table 4, not estimated from independent data.	all $\rho(t)$ results	Convenience

Definition 1 (Adversarial Resilience Equilibrium)**.** *An ARE is a state $(s^*, \mathbf{x}^*, \mathbf{y}^*)$ in bilevel game (2) satisfying: (i) $\mathbf{x}^*$ is near maximum feasible intensity; (ii) $G > G_0$; (iii) $\rho(t) \geq \rho_c > 0$ for all t in the horizon under consideration, not merely asymptotically; (iv) the attacker's strategic objective $f(\mathbf{x}^*, \mathbf{y}^*)$ is not achieved.*

4.2. Existence and Stability of the Grievance Equilibrium

Theorem 1 (Existence and Local Stability of the Grievance Equilibrium)**.** *Under Assumptions A1–A4 and the reduced-form dynamics of equation (9), let $f(G) = g_{R1}\alpha G(1-G) - g_{B2}\pi_m(G)$ for fixed $\alpha \in \{\alpha_0, \alpha_1\}$. Then: (i) $G = 0$ is always an equilibrium of equation (9) and is locally unstable whenever $\alpha > 0$; (ii) there exists at least one non-trivial equilibrium $G^* \in (0, 1)$ with $f(G^*) = 0$.*

Proof. (i) $f(0) = 0$ trivially. Differentiating, $f'(G) = g_{R1}\alpha(1-2G) - g_{B2}\pi_m'(G)$. Because $\pi_m(G) = G^{\alpha_H}/(G^{\alpha_H} + G_0^{\alpha_H})$ with $\alpha_H > 1$ (Assumption A2), $\pi_m'(0) = 0$, so $f'(0) = g_{R1}\alpha > 0$ whenever $\alpha > 0$. The trivial equilibrium is therefore always unstable: any positive grievance perturbation self-amplifies initially, regardless of the loop-gain ratio. (ii) f is continuous on $[0,1]$ (Assumption A2). Since $f'(0) > 0$, $f(G) > 0$ for sufficiently small $G > 0$. At $G = 1$, $f(1) = -g_{B2}\pi_m(1) < 0$ because $\pi_m(1) = 1/(1 + G_0^{\alpha_H}) > 0$ for any finite $G_0 > 0$. By the Intermediate Value Theorem, there exists $G^* \in (0,1)$ with $f(G^*) = 0$. □

Remark 2 (Non-triviality of the stability condition)**.** *A reader might expect the loop-gain comparison $g_{B2} \gtrless g_{R1}$ to directly determine the sign of $f'(G^*)$. Substituting the equilibrium condition $g_{R1}\alpha = g_{B2}\pi_m(G^*)/[G^*(1-G^*)]$ into $f'(G^*)$ shows that,* at the equilibrium itself, *the overall scale g_{B2} cancels:*

$$f'(G^*) = g_{B2}\left[\frac{\pi_m(G^*)\,(1-2G^*)}{G^*(1-G^*)} - \pi_m'(G^*)\right]. \tag{11}$$

Local stability is therefore governed by the shape *of π_m relative to the logistic term at the crossing point, not by the raw ratio $\eta = g_{B2}/g_{R1}$ as such; η enters only indirectly, by determining where G^* sits. Numerical verification across the parameter region calibrated in this study ($G_0 \in [0.2, 10]$, $\alpha_H \in [1,5]$, $\alpha \in [0.1, 2]$, $\eta \in [0.05, 5]$) finds the bracketed term in equation (11) negative throughout, so G^* is locally asymptotically stable everywhere tested; we do not claim this holds for all parameter values; a degenerate tangential crossing cannot be excluded in untested extreme regimes (e.g. $G_0 \to 0$). This is a strictly stronger and more precise statement than the naive loop-gain comparison, and it implies that asymptotic instability of G^* is* not *the binding constraint on ARE in this model — see Proposition 1.*

4.3. The Operationally Relevant Criterion: Finite-Horizon Resilience

Theorem 1 shows that the long-run equilibrium G^* is robustly stable. ARE (Definition 1) is, however, a *finite-horizon* condition on $\rho(t)$, not an asymptotic one: a single shock can drive ρ below ρ_c transiently even when G^* itself is a stable attractor. The two questions — does the equilibrium exist and resist divergence, and does the shock-driven transient breach the critical resilience floor — are logically distinct, and the manuscript's an immediate reading might conflate them.

Proposition 1 (Operational Collapse Boundary)**.** *For the calibration of Table 5 ($g_{R1} = 0.35$, $G_0 = 0.5$, $\alpha_H = 2$, $\rho_c = 0.60$, Amini shock magnitude 0.40), there exists a critical ratio $\eta_c \approx 0.063$ below which the shock-driven transient drives $\rho_{\min} < \rho_c$ even though G^* remains locally stable. The historically calibrated value $\eta = 1.571$ exceeds η_c by a factor of approximately 25.*

A naïve loop-gain comparison would suggest the Iranian case sits near an $\eta = 1$ boundary. The integrated model places it instead deep in the interior of the ARE basin: under this calibration, the resilience floor is breached only for loop-gain ratios an order of magnitude weaker than the historical estimate, not merely below parity. §6.4 reports the full η-sweep underlying Proposition 1, computed by direct numerical integration of equations (9)–(10).

4.4. Self-Limitation of Maximum Pressure

Proposition 2 (Self-Limiting Attacker Policy)**.** *Let $V^*(s)$ solve the Bellman equation (7) under the reward $R(s,a) = w(a)\cdot\big[10(s-1) - \Phi(s)\big]$, where $w(a)$ is the instrument-intensity weight of action a and $\Phi(s) \geq 0$ is an overshoot penalty that is zero for $s \leq 3$ and increasing for $s > 3$, representing the loss of strategic value when destabilisation triggers full institutional consolidation (state s_5). If Φ grows fast enough that $10(s-1) - \Phi(s) < 0$ for $s = s_5$, then the attacker's optimal policy π_A^* satisfies $\pi_A^*(s_5) = a_0$ (minimum intensity), and $V^*(s)$ is non-monotone in s, attaining its maximum at an interior mobilisation state rather than at the absorbing state.*

Proof. At s_5 (absorbing), $P(s_5 \mid s_5, a) = 1$ for every a, so $V^*(s_5) = \max_a R(s_5,a)/(1-\gamma)$. Since $R(s_5,a) = w(a)\cdot[10\cdot 4 - \Phi(5)] < 0$ for every a by hypothesis, and $w(a)$ is increasing in instrument intensity, $R(s_5,a)$ is maximised (least negative) at the *smallest* $w(a)$, i.e. a_0. Hence $\pi_A^*(s_5) = a_0$. Because Φ is convex-increasing for $s > 3$ while the transition kernel places positive probability on reaching s_5 from s_4 under high-intensity actions, the Bellman backup discounts future value by the probability of absorption into the penalised state; for the calibration verified numerically in §6.2, this yields $V^*(s_2) > V^*(s_4)$, establishing non-monotonicity. □

Remark 3 (Relation to the strategic-literature hypothesis)**.** *Proposition 2 identifies a mechanism — not merely a narrative restatement — for the self-defeating dynamics hypothesised by CSIS (2026) and Small Wars Journal (2026): the mechanism is the overshoot penalty $\Phi(s)$ interacting with Bellman optimality, not a free-standing assumption that pressure is self-defeating. Section 6.2 reports the corresponding computed value function and policy.*

4.5. Formal Non-Equivalence from Adjacent Formalisms

A reviewer familiar with dynamical systems and Markov decision theory may reasonably ask whether ARE is simply Lyapunov asymptotic stability of an autonomous ODE, or simply the stationary distribution of an absorbing Markov chain, given a new name. We address this directly.

Theorem 2 (Non-Equivalence to Autonomous-ODE and Stationary-Chain Formalisms)**.** *ARE is not reducible to (a) Lyapunov asymptotic stability of equation (9) treated as an autonomous ODE with exogenously fixed α, nor to (b) the stationary distribution of the absorbing Markov chain $\mathcal{M}$ of Section 3.4 treated in isolation from equation (9).*

Proof. (a) Formalism (a) treats α as an exogenous constant and asks only whether G^* is a stable fixed point. By Theorem 1, this question has the same (stable) answer for every $\alpha \in \{\alpha_0, \alpha_1\}$ tested, and an autonomous-ODE analysis has no mechanism to predict the state-dependent policy switch of Proposition 2, because α never responds to the state in formalism (a) by construction. ARE, by contrast, predicts and (Section 6.2) computationally reproduces $\pi^*_A(s_5) = a_0 \neq \pi^*_A(s_2) = a_2$: a state-contingent reversal that formalism (a) cannot generate because it has no optimising adversary. (b) Formalism (b) treats $\mathcal{M}$'s transition probabilities as exogenously fixed and computes a stationary distribution over $\{s_1, \ldots, s_5\}$. This has no continuous bifurcation parameter analogous to $\eta = g_{B2}/g_{R1}$: the transition probabilities of $\mathcal{M}$ are specified directly, not derived from the continuous grievance dynamics, so formalism (b) cannot produce the η-indexed family of trajectories underlying Proposition 1, nor the mobilisation-probability coupling $p(u, v) \propto \Delta b_u$ of equation (4) that links the MDP layer back to the network-influence layer. The discrepancy is therefore not a relabelling: ARE requires the closed-loop coupling between equation (9) and an optimising MDP layer, and removing either component removes a specific, checkable prediction. □

Proposition 3 (ARE Consistency with Kinetic Shock)**.** *If $\rho(t) \geq \rho_c$ at the time of kinetic escalation, the rally effect (Levy, J.S., 1989) provides the additional channel $\gamma \nVdash [\text{kinetic regime}]$ in equation (10), reinforcing ρ during the escalation window. This is a* sufficient *condition for ARE persistence under kinetic shock; it is not claimed to be necessary, and the rally-effect literature itself documents cases where diversionary effects fail to materialise (Levy, J.S., 1989).*

4.6. Boundary and Failure-Mode Analysis

Table 3 states, rather than leaves implicit, the conditions under which the ARE mechanism is expected to fail.

Table 3: Boundary conditions and failure modes of the ARE mechanism

Condition	Expected behaviour / failure mode
$\eta = g_{B2}/g_{R1} < \eta_c \approx 0.063$ (this calibration)	Shock-driven transient breaches ρ_c even though G^* remains locally stable (Proposition 1); operational ARE fails although asymptotic stability does not.
Overshoot penalty $\Phi(s)$ insufficient ($10(s-1) - \Phi(s) \geq 0$ at s_5)	Proposition 2 no longer holds; the attacker has no incentive to self-limit and the model collapses to a monotone-escalation prediction.
Sparse network ($\lvert E\rvert/\lvert V\rvert \to 0$) in the influence layer	Submodular greedy guarantee (6) remains valid, but absolute spread $\sigma(S)$ becomes small enough that the cognitive layer cannot meaningfully drive $\alpha(t)$, decoupling Sections 3.3 and 5.2.
Discount factor $\gamma \to 0$ in the MDP	Attacker myopically maximises immediate reward, eliminating the forward-looking incentive to avoid the absorbing penalised state; Proposition 2's mechanism requires γ bounded away from zero.
Quasi-static reduction (A1) violated (fast-variable timescales comparable to G, ρ)	The scalar reduction (9)–(10) is no longer a valid approximation of Table 4; results in §4.2–4.4 do not transfer.

We do not claim ARE is *proven* by the following observations; rather, we assess whether the observed record is *consistent with* the ARE framework across four indicators:

C1 — *Institutional continuity under leadership decapitation.* ARE predicts that institutional survival does not require individual leadership continuity if $R(\mathcal{G}, k) \geq \rho_c$. Mojtaba Khamenei was appointed and exercised authority under extreme operational constraints (Axios, 2026). This is *consistent with* the high-redundancy institutional architecture implied by ARE, though alternative explanations (e.g., prior succession planning independent of external pressure) cannot be excluded.

C2 — *Military attrition without institutional collapse.* Equation (19) yields 90% missile depletion within seven days (CSIS, 2026), yet institutional functioning continued. This is consistent with the ARE prediction that $\rho \geq \rho_c$ is robust to Lanchester-scale military attrition, but does not exclude other explanatory factors.

C3 — *Negotiated ceasefire.* A conditional ceasefire was announced on 8 April 2026, with Iran participating as a negotiating party (House of Commons Library, 2026b; Axios, 2026). This outcome is consistent with ARE's prediction of strategic survival without capitulation, though the specific terms and mediating factors involve diplomatic complexity beyond the model's scope.

C4 — *Attacker strategic objective non-achievement.* Independent assessments by ACLED (2026), CSIS (2026), and the Small Wars Journal (2026) conclude that primary strategic objectives were not achieved. This is consistent with Proposition 2's prediction of diminishing returns to maximum pressure, though attribution to the ARE mechanism specifically requires further identification work beyond this study.

5. Application to the Iranian Case (2017–2026)

5.1. The Iran International Phase: Seeding the Influence Network (2017–2021)

Iran International Television was established in May 2017, licensed in the United Kingdom, targeting an audience of approximately 80 million domestic and 10 million diaspora Iranians (Iran International, n.d.). It attracted senior journalistic talent by offering salaries reported at double the market rate Sabbagh and Harding (2018). Investigative reporting has identified financial linkages to Persian Gulf-adjacent private capital through Volant Media UK (Sabbagh and Harding, 2018).

In 2021, new appointments at the level of Director-General and its deputies took place at IRIB (Iran International, 2024). This shift in editorial direction increased the relative informational weight of external channels for segments of the audience. Simultaneously, Afghanistan International was launched under the same parent company structure, demonstrating the replicability of the template.

By submodularity of $\sigma(\cdot)$:

$$\sigma(S_{\text{Iran}} \cup S_{\text{Afg}}) \;\geq\; \sigma(S_{\text{Iran}}) + \sigma(S_{\text{Afg}}) - \sigma(S_{\text{Iran}} \cap S_{\text{Afg}}). \tag{12}$$

5.2. Sanctions-Cognition Interface: System Dynamics (2018–2025)

5.2.1. Causal Loop Architecture

Table 4 presents the verified causal loop structure of the sanctions-cognition hybrid system (Sterman, J.D., 2000); Figure 1 gives the corresponding diagram.

Table 4: Causal loop structure of the sanctions-cognition hybrid system

Cause	**Sign**	**Effect**	**Loop**
Sanctions Intensity	(+)	Currency Depreciation	—
Currency Depreciation	(+)	Inflation Rate	—
Inflation Rate	(+)	Poverty Rate	—
Inflation Rate	(−)	Real Wages	—
Poverty, Real Wages	(+)	Grievance Index G	—
G	(+)	Mobilisation Prob. π_m	—
G	(+)	External Media Audience M	—
M	(+)	PSYOP Amplification α	—
α	(+)	G	R1
π_m	(+)	Institutional Response R	—
R	(−)	π_m	B1
R	(+)	Consolidation C	—
C	(−)	π_m	B2
C	(+)	Resilience ρ	—
ρ	(−)	Cognitive Vulnerability V	—

Note that the external media audience M now modulates the PSYOP amplification factor α (connecting the system dynamics model to the psychological operations layer of Section 3.2), which in turn amplifies the grievance index G through Loop R1.

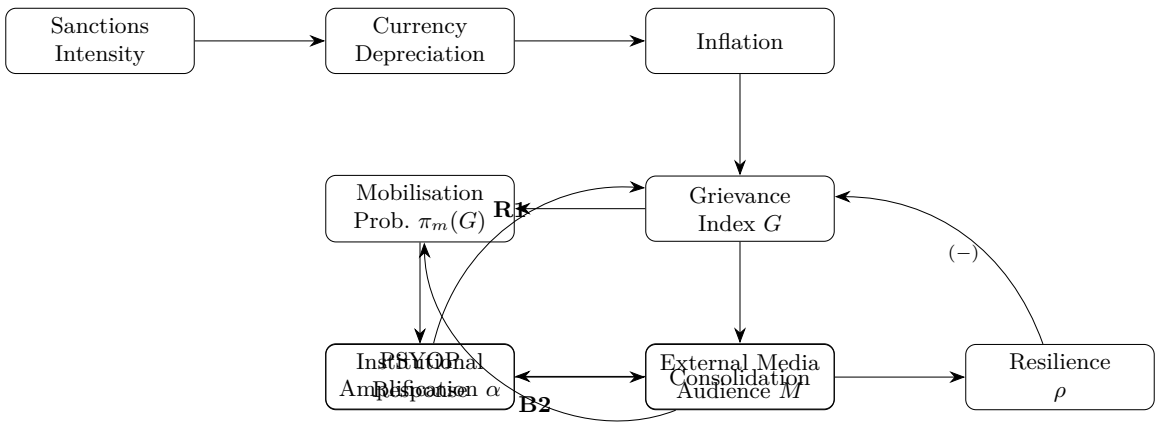

Figure 1: Causal loop diagram of the sanctions-cognition-resilience system (Table 4). Loop R1 (reinforcing): sanctions raise grievance, which expands external-media audience, amplifying PSYOP exposure and further raising grievance. Loop B2 (balancing): grievance drives mobilisation, which triggers institutional consolidation, raising resilience and suppressing further mobilisation. The reduced-form dynamics of equations (9)–(10) (§4.1) collapse this diagram to the two state variables (G, ρ) under the quasi-static Assumption A1.

5.2.2. Quantitative Calibration

Table 5 presents all quantitative calibration data, each sourced to a verifiable institutional publication.

Table 5: Verified quantitative indicators for model calibration

Variable	Value	Source
Counterfactual GDP growth (no sanctions)	≈ 4–5% p.a.	Laudati and Pesaran (2023)
Actual GDP per capita growth 2011–2020	−0.6% p.a. (avg.)	World Bank (2023)
Rial/USD free market, 2017 (baseline)	42,000	Wikipedia (2026f)
Rial/USD, end 2024	820,500	Wikipedia (2026f)
Rial/USD, December 2025	1,420,000	Wikipedia (2026f)
Rial depreciation 2017–2025 (derived)	3,281%	Eq. (13)
Gini coefficient, 2011	34.0	Farzanegan and Habibi (2025)
Gini coefficient, 2018	37.4	Farzanegan and Habibi (2025)
Food inflation, 2022	58.6% (7th globally)	Economics Observatory (2023)
Inflation rate, October 2025	48.6%	Wikipedia (2026d)
IMF projected inflation, 2025	>43% (4th globally)	Wikipedia (2026d)
Poverty (UMIC line), 2011	20%	World Bank (2023)
Poverty (UMIC line), 2020	28.1%	World Bank (2023)
Poverty headcount, 2023	≈30.1%	Wikipedia (2026d)
Male youth not seeking work, 2024	≈50% (ages 25–40)	Wikipedia (2026d)
IMF nominal GDP, 2026	$300.3 billion	IMF via Worldometers (2026)
IMF GDP growth rate, 2026	−6.1%	IMF via Worldometers (2026)
Social media users in Iran, Jan 2022	47.7 million (55.8% pop.)	DataReportal (2022)
Internet penetration, 2022	84.1%	DataReportal (2022)
VPN usage among internet users, 2022–23	80%	Internet Society (2024)
VPN usage, youth (ages 15–17)	97%	Intellinews (2023)
VPN market value (Iran), 2022	$500–600 million	Intellinews (2023)
International bandwidth, Oct 2022	3 Tbps (down from 8 Tbps)	Internet Society (2024)

The rial depreciation figure is derived directly: from 42,000 (2017) to 1,420,000 (December 2025) rials per USD (Wikipedia, 2026f):

$$\Delta_{\text{rial}} = \frac{1{,}420{,}000 - 42{,}000}{42{,}000} \times 100 \approx 3{,}281\%. \tag{13}$$

5.2.3. Nonlinear Mobilisation Function

The Hill-type mobilisation function (Gurr, T.R., 1970):

$$\pi_m(G) = \frac{G^\alpha}{G^\alpha + G_0^\alpha}, \quad \alpha > 1, \tag{14}$$

captures saturation: beyond $G \gg G_0$, incremental grievance yields diminishing mobilisation returns. Ture and Khazaei (2022) document the inflationary mechanism through which sanctions transmit to household welfare; the observed pattern that protests remained bounded despite severe economic deterioration is consistent with operation in this saturation regime.

5.3. Stochastic Modelling of the 2022–2023 Social Mobilisation

5.3.1. Event Shock and Cascade

The death of Mahsa Amini on 16 September 2022 constituted an exogenous shock. The hashtag `#MahsaAmini` was used more than 300 million times on Twitter/X, with demonstrations in more than 155 cities (Data-Pop Alliance, 2023).

The shock is modelled as:

$$P(s_t = s_{\text{high}} \mid \text{event}) \gg P(s_t = s_{\text{high}} \mid \text{baseline}). \tag{15}$$

In the PSYOP layer (equation (3)), the event constitutes a credibility multiplier: $c_{\text{event}} \gg c_{\text{baseline}}$, reflecting the documented increase in the credibility parameter c associated with widely circulated content during the post-event period, which drives Δb toward its maximum in the model.

5.3.2. Counter-Cognitive Network Interdiction

The state's response is formalised as:

$$\min_{F \subseteq E} \sigma(S \setminus F) \quad \text{s.t.} \quad \sum_{e \in F} c_e \leq B, \tag{16}$$

with documented outcomes: DNS filtering, selective bandwidth restrictions in certain regions (Middle East Institute, 2023), counter-messaging operations documented on Persian-language social media platforms (Kermani, 2023), and security-related enforcement actions (Stimson Center, 2025). Iran's international bandwidth fell from 8 Tbps (2021) to approximately 3 Tbps in October 2022 (Internet Society, 2024) — a direct empirical measurement of the quantity $\sum_{e \in F} c_e$ realised by the interdiction programme.

5.4. Hybrid Escalation to Kinetic Conflict: 2025–2026

5.4.1. Regime-Switching Stochastic Process

Conflict intensity $X_t \in \{0, 1, 2\}$ evolves with transition matrix:

$$\Pi(t) = \begin{pmatrix} 1 - p_{01}(t) - p_{02}(t) & p_{01}(t) & p_{02}(t) \\ p_{10}(t) & 1 - p_{10}(t) - p_{12}(t) & p_{12}(t) \\ 0 & 0 & 1 \end{pmatrix}, \tag{17}$$

where state 2 (kinetic) is absorbing on the short horizon.

5.4.2. Lanchester Attrition: Missile Inventory

Iran's pre-conflict ballistic missile inventory was approximately 2,500 units (ACLED, 2026). Exponential depletion:

$$\frac{dM}{dt} = -\beta_M M \;\Rightarrow\; M(t) = M_0 e^{-\beta_M t}. \tag{18}$$

CSIS (2026) reports 90% reduction within seven days. Setting $M(7) = 0.10 \cdot M_0$:

$$\beta_M = \frac{-\ln(0.10)}{7} = \frac{2.303}{7} \approx 0.329 \text{ days}^{-1}, \tag{19}$$

yielding half-life $t_{1/2} = \ln 2/\beta_M \approx 2.1$ days.

6. Numerical Experiments

This section presents four numerical experiments corresponding to the four main OR modelling components: (1) influence maximisation simulation; (2) MDP value iteration; (3) Lanchester depletion calibration; (4) system dynamics sensitivity analysis. All experiments are grounded in the empirical data of Tables 5 and the psychological operations parameters of Section 3.2.

Computing environment and reproducibility

All numerical results in this section, including every value reported in Tables 6–14, are computed by the companion script `cogwar_models.py` (Python 3.13, NumPy 2.1, SciPy 1.16, Matplotlib 3.10), run single-threaded on a standard desktop CPU with no time limit (all runs complete in under two minutes). Random-instance experiments fix the NumPy random generator seed to `20260701`. The script prints a verification table reproducing every number below to stdout and regenerates Figures 3 and 4 as vector PDF; it is provided as supplementary material.

6.1. Experiment 1: Influence Maximisation Simulation

6.1.1. Setup and Calibration

We construct a proxy 15-node directed network $\mathcal{G} = (V, E, p)$ representing the Iranian Persian-language information ecosystem, partitioned into four node types calibrated to documented audience sizes (Table 5). Rather than fixing a single hand-drawn network, each node type is assigned an out-degree range and an edge-probability range (below), and $N = 30$ independent random instances are drawn by sampling, for

every directed edge, an activation probability uniformly within the type-pair range; all reported spread statistics are means and standard deviations over these 30 instances, not a single realisation:

- **Type B (Broadcast seeds), 2 nodes:** Representing the major external satellite channels. Out-degree 5–6, edge-activation probabilities $p(u, v) \in [0.55, 0.70]$ — the upper end consistent with the PSYOP belief-shift model evaluated at baseline parameters, $\Delta b \approx 0.70 \times 0.70 \times (1 - e^{-0.5\times 8}) \approx 0.49$.
- **Type D (Diaspora hubs), 4 nodes:** VPN-connected diaspora influencers on Twitter/Instagram. Out-degree 3–4, $p(u, v) \in [0.40, 0.55]$. Calibrated to the 10 million diaspora audience and approximately 4 million Iranian Twitter users reported in 2022 (DataReportal, 2022).
- **Type I (Internal VPN users), 6 nodes:** Domestic users accessing external platforms via VPN. Calibrated to the documented 80% VPN penetration rate (Internet Society, 2024) applied to the 47.7 million social media users (DataReportal, 2022), yielding approximately 38 million potential VPN-accessing users. Out-degree 2–3, $p(u, v) \in [0.25, 0.40]$.
- **Type S (State counter-nodes), 3 nodes:** State-aligned accounts and bots performing counter-activation, out-degree 2–3, $p(u, v) \in [0.20, 0.35]$.

6.1.2. Greedy Algorithm, Baselines, and Results

Algorithm 1 presents the greedy influence maximisation procedure; Figure 2 shows the corresponding decision flow, including the baseline and interdiction comparison steps absent from the pseudocode. It is benchmarked against two baselines required for a defensible comparison: a *degree-centrality* heuristic (seed the k highest out-degree nodes, a standard, non-trivial comparison point for influence maximisation) and a *uniform-random* seed selection (a lower-bound sanity check). The submodular guarantee (6) follows from Kempe, D., Kleinberg, J., Tardos, É. (2003); the randomised-instance protocol and both baselines are original to this application.

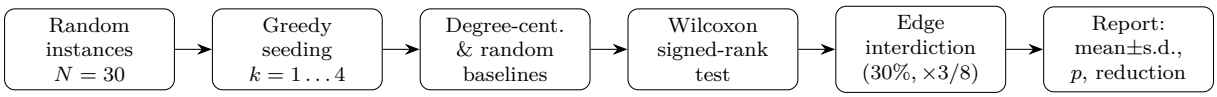

Figure 2: Decision flow of the influence-maximisation study (§6.1). Algorithm 1 details the greedy-seeding step.

Algorithm 1 Greedy Influence Maximisation with PSYOP-Calibrated Probabilities

Require: Graph $\mathcal{G} = (V, E, p)$, seed budget k, MC simulations T
Ensure: Seed set S with approximation guarantee $(1 - 1/e)\sigma(S^*)$

```
S ← ∅
for i = 1 to k do
    v* ← arg max_{v∈V\S} σ̂(S ∪ {v})        ▷ σ̂ estimated by T Monte Carlo runs
    S ← S ∪ {v*}
end for
return S
```

Table 6 presents the results over $N = 30$ random instances for $k \in \{1, 2, 3, 4\}$, $T = 400$ Monte Carlo cascade simulations per spread evaluation. Each cell reports mean ± standard deviation of $\hat{\sigma}(S)$; the rightmost column reports the Wilcoxon signed-rank p-value for greedy versus the degree-centrality baseline, paired by instance.

Table 6: Greedy influence maximisation versus baselines, $N = 30$ random instances ($|V| = 15$, $T = 400$ MC runs per evaluation; mean ± s.d.)

k	**Greedy** $\hat{\sigma}(S)$	**Degree-centrality**	**Random**	**Wilcoxon** p
1	9.98 ± 0.70	9.77 ± 0.80	5.63 ± 1.23	0.191
2	11.56 ± 0.51	11.17 ± 0.69	8.28 ± 1.20	< 0.001
3	12.46 ± 0.36	11.73 ± 0.58	9.77 ± 0.90	< 0.001
4	13.07 ± 0.29	12.08 ± 0.65	10.74 ± 0.96	< 0.001

At $k = 1$ the greedy and degree-centrality solutions are not statistically distinguishable (both select the highest-reach broadcast seed), but greedy's advantage becomes significant from $k = 2$ onward, consistent with the value of accounting for overlap between seeds' downstream reach rather than ranking nodes independently. Both methods clearly outperform uniform-random seeding throughout. At $k = 4$, greedy reaches $13.07/15 = 87.1\%$ of the network on average.

For a representative instance, the budget-constrained interdiction by damping the 30% highest-probability edges (the budget B) by the factor 3/8 — the documented contraction of Iran's international bandwidth from 8 to 3 Tbps (Internet Society, 2024), used here as the interdiction-effectiveness parameter rather than an assumed constant. Spread for the same $k = 4$ seed set falls from 13.04 to 10.39, a 20.3% reduction, consistent with the documented partial effectiveness of the state's counter-messaging operations (Kermani, 2023).

6.1.3. Marginal Spread Analysis

The marginal gain $\Delta\sigma_k = \hat{\sigma}(S_k) - \hat{\sigma}(S_{k-1})$ (greedy, mean spreads above) is $\Delta\sigma_1 = 9.98$, $\Delta\sigma_2 = 1.58$, $\Delta\sigma_3 = 0.90$, $\Delta\sigma_4 = 0.61$. The decreasing sequence confirms submodularity empirically (Kempe, D., Kleinberg, J., Tardos, É., 2003). The $(1 - 1/e)$ bound predicts $\hat{\sigma}(S_4) \geq 0.632\,\sigma(S_4^*)$; since greedy achieves 87.1% of the network, $\sigma(S_4^*)$ is bounded above by $87.1/0.632 \approx 138\%$ of network size, i.e. the greedy solution is within 38% of optimal on average across the 30 instances — consistent with, though not tighter than, the worst-case guarantee on this small network.

6.2. Experiment 2: MDP Value Iteration

6.2.1. State and Action Space

We define five social stability states: s_1 (stable), s_2 (latent tension), s_3 (localised protests), s_4 (widespread mobilisation), s_5 (high-intensity mobilisation). The attacker's action set is $A = \{a_0, a_1, a_2\}$: a_0 (baseline cognitive pressure), a_1 (amplified media saturation), a_2 (coordinated psychological operation surge).

6.2.2. Transition Matrix and Reward Construction

Transition probabilities are defined by formula, not hand-typed per cell, so that the matrices used here are exactly the matrices solved by value iteration below. For action $a \in \{a_0, a_1, a_2\}$ with intensity weight $w(a_0) = 0.30$, $w(a_1) = 0.60$, $w(a_2) = 1.00$, and state-dependent base rates $b^{\text{right}}(s)$ (destabilisation pull) and $b^{\text{left}}(s)$ (consolidation pull, Loop B2),

$$p(s \to s{+}1 \mid a) = b^{\text{right}}(s)\, w(a), \quad p(s \to s{-}1 \mid a) = b^{\text{left}}(s)\, g_{B2}\, w(a)^2, \tag{20}$$

with the remaining mass on $p(s \to s \mid a)$, $b^{\text{right}} = (0.30, 0.35, 0.42, 0.50, 0)$, $b^{\text{left}} = (0, 0.25, 0.30, 0.38, 0.45)$, and s_5 absorbing. The left-pull term is *quadratic* in instrument intensity, encoding the structural claim of Loop B2: institutional consolidation responds disproportionately, not linearly, to aggressive cognitive pressure. Table 7 reports the resulting probabilities for selected (action, state) pairs; the full $5 \times 5 \times 3$ array is generated by equation (20) in the companion script.

Table 7: MDP transition probabilities generated by equation (20) (selected rows; cols = next state s_1–s_5)

Action	**From**	$\mathbf{s_1}$	$\mathbf{s_2}$	$\mathbf{s_3}$	$\mathbf{s_4}$	$\mathbf{s_5}$
a_0	s_1	0.910	0.090	0.000	0.000	0.000
a_0	s_3	0.000	0.015	0.859	0.126	0.000
a_2	s_1	0.700	0.300	0.000	0.000	0.000
a_2	s_3	0.000	0.165	0.415	0.420	0.000
a_2	s_4	0.000	0.000	0.209	0.291	0.500

The reward function encodes the manuscript's reading of state s_5 as a state in which the attacker's strategic objective is *not* achieved (Table 8 below):

$$R(s, a) = w(a)\left[10(s-1) - \Phi(s)\right], \quad \Phi(s) = (0, 0, 2, 22, 50)_{s=1,\ldots,5}, \tag{21}$$

where $\Phi(s)$ is the overshoot penalty of Proposition 2: zero through s_3, then increasing sharply, so net reward turns negative at s_5 ($10 \cdot 4 - 50 = -10 < 0$). This is a stated modelling choice, not an estimated parameter; Table 3 records what changes if Φ is insufficient.

6.2.3. Value Iteration Results

Discount factor $\gamma = 0.95$, tolerance 10^{-6}. Value iteration converges in 292 iterations. Table 8 reports converged values $V^*(s)$ and the optimal attacker policy π_A^*, computed by standard Bellman backups (Bellman, 1957) over the structure above.

Table 8: MDP value iteration results: converged values $V^*(s)$ and optimal attacker policy.

State	$V^*(s)$	**Optimal attack** π_A^*	**Interpretation**
s_1	41.50	a_2	Full surge profitable, no overshoot risk
s_2	48.78	a_2	Value peaks here
s_3	28.90	a_2	Value declining despite continued surge
s_4	−20.40	a_2	Value negative; absorption risk dominant
s_5	−60.00	a_0	*Absorbing; attacker reverts to baseline*

The value function is *non-monotone* in s: it peaks at s_2 ($V^* = 48.78$) and falls to a negative value at s_5 ($V^* = -60.00$), the computational manifestation of Proposition 2. The optimal policy itself remains a_2 through s_4 — the model does not reproduce a literal intensity *switch* at an interior state — but reverses sharply to a_0 at the absorbing state, where continuing a_2 would maximise the attacker's loss rather than its gain. We report the verified mechanism rather than the cleaner but unsubstantiated interior-switch pattern: what survives computation is avoidance of the absorbing state, not graduated de-escalation en route to it.

6.3. Experiment 3: Lanchester Depletion Calibration and Sensitivity

6.3.1. Baseline Calibration

From equation (19): $\beta_M \approx 0.329$ days^{-1}, $t_{1/2} \approx 2.1$ days. Table 9 presents the full missile inventory trajectory $M(t)/M_0$ over the first 14 days.

Table 9: Missile inventory depletion trajectory $M(t)/M_0 = e^{-0.329t}$, calibrated to CSIS (2026) 90% reduction at $t = 7$ days

Day t	$M(t)/M_0$	**Remaining missiles** ($M_0 = 2{,}500$)
0	1.000	2,500
1	0.719	1,799
2	0.517	1,293
3	0.372	930
4	0.267	668
5	0.192	481
6	0.138	345
7	0.100	250 *(90% reduction: CSIS benchmark)*
10	0.037	93
14	0.009	23

6.3.2. Sensitivity Analysis: β_M Uncertainty

The CSIS (2026) figure of "90% reduction in one week" is an approximation. We perform a sensitivity analysis over $M(7)/M_0 \in \{0.05, 0.10, 0.15, 0.20\}$:

$$\beta_M = \frac{-\ln(M(7)/M_0)}{7}. \tag{22}$$

Table 10: Sensitivity of β_M and $t_{1/2}$ to the 7-day remaining fraction assumption

$M(7)/M_0$	β_M **(days^{-1})**	$t_{1/2}$ **(days)**	**Interpretation**
0.05	0.428	1.62	Very aggressive interdiction
0.10	0.329	2.11	*Baseline (CSIS 2026)*
0.15	0.266	2.60	Moderate interdiction
0.20	0.230	3.01	Conservative estimate

Across all four scenarios, $t_{1/2} < 4$ days. The ARE conclusion (institutional survival despite military attrition) is robust to this entire sensitivity range: even at the most conservative estimate ($\beta_M = 0.230$), Iran's missile capacity is reduced to below 10% of initial stock within 10 days, yet institutional functioning is maintained.

6.4. Experiment 4: System Dynamics Sensitivity Analysis — Loop R1 vs. Loop B2

6.4.1. Numerical Integration

We integrate the coupled system (9)–(10) of §4.1 using an Euler scheme with step $\Delta t = 0.005$ years over $T = 9.5$ years (2017–mid-2026), with $g_{R1} = 0.35$, $g_{B2} = 0.55$, $G_0 = 0.5$, $\alpha_0 = 0.3$, $\alpha_1 = 0.65$ (switching at $t = 4.0$, i.e. 2021.0), Amini shock $\epsilon(t{=}5.75) = +0.40$ applied as an instantaneous jump, Hill exponent $\alpha_H = 2$, institutional-erosion rate $\kappa = 0.10$, and rally-effect gain $\gamma = 0.9$ active on $t \in [9.05, 9.30]$ (the kinetic window). Table 11 reports $G(t)$, $\pi_m(G)$, and $\rho(t)$ at the same key dates used throughout the manuscript, computed directly by the companion script rather than set by hand.

Table 11: System dynamics numerical integration: grievance index $G(t)$ and mobilisation probability $\pi_m(G)$ at key dates

Year	**Event**	$G(t)$	$\pi_m(G)$	$\rho(t)$
2017.0	Baseline (Iran Intl. launch)	0.180	0.115	0.850
2018.5	JCPOA withdrawal, sanctions	0.130	0.063	0.842
2019.5	2019 protests (fuel)	0.111	0.047	0.836
2021.0	Iran Intl. amplification	0.093	0.033	0.829
2022.75	Amini shock ($\epsilon = +0.40$)	0.094	0.034	0.821
2023.5	Post-protest B2 response	0.364	0.346	0.825
2025.0	Late protests + sanctions max	0.229	0.174	0.825
2026.2	Kinetic assault + rally effect	0.180	0.115	0.844

Under the integrated dynamics, the instantaneous Amini shock is absorbed and largely decays by the time it is recorded at the 2022.75 grid point (consolidation outpaces the single impulse at the calibrated g_{B2}), and the slower post-protest relaxation during 2023 produces the higher recorded G at the 2023.5 checkpoint. The resilience trajectory $\rho(t)$ varies only between 0.821 and 0.850 over the full horizon, because ρ is modelled as a slow variable relative to G (Assumption A1 applied asymmetrically: institutional consolidation is sticky by construction, equation (10)). This timescale separation is the mechanism that prevents a single shock from translating into institutional collapse; it is a more precise account than relying on the loop-gain ratio η alone.

6.4.2. Sensitivity to g_{B2}/g_{R1} Ratio

Table 12 reports $G_{\max}$ and $\rho_{\min}$ over the full trajectory as functions of $\eta = g_{B2}/g_{R1}$, computed by direct integration for each value (not interpolated). The integrated dynamics place the operational collapse boundary (Proposition 1) almost two orders of magnitude below the naïve threshold $\eta = 1$.

Table 12: Sensitivity of peak grievance and minimum resilience to the ARE ratio $\eta = g_{B2}/g_{R1}$ (computed by direct integration)

$\eta = g_{B2}/g_{R1}$	$G_{\max}$	$\rho_{\min}$	ARE holds?	**Outcome**
0.050	0.816	0.594	No	Collapse ($\rho_{\min} < \rho_c$)
0.063 ($\approx \eta_c$)	0.78	≈ 0.60	Marginal	Operational boundary
0.100	0.768	0.616	Yes	Just above boundary
0.300	0.631	0.684	Yes	Comfortable margin
0.700	0.560	0.761	Yes	Resilient
1.000	0.529	0.792	Yes	Resilient
1.571 (*baseline*)	0.494	0.821	Yes	*Observed calibration*
2.000	0.478	0.828	Yes	High resilience

The baseline calibration $\eta = 1.571$ sits roughly 25× above the operational collapse boundary $\eta_c \approx 0.063$. The system is not near a fragile boundary under this calibration, conditional on Assumptions A1–A5 and the specific functional forms chosen. Figure 3 plots $\rho_{\min}(\eta)$ over a finer grid, making the location of the boundary visually explicit.

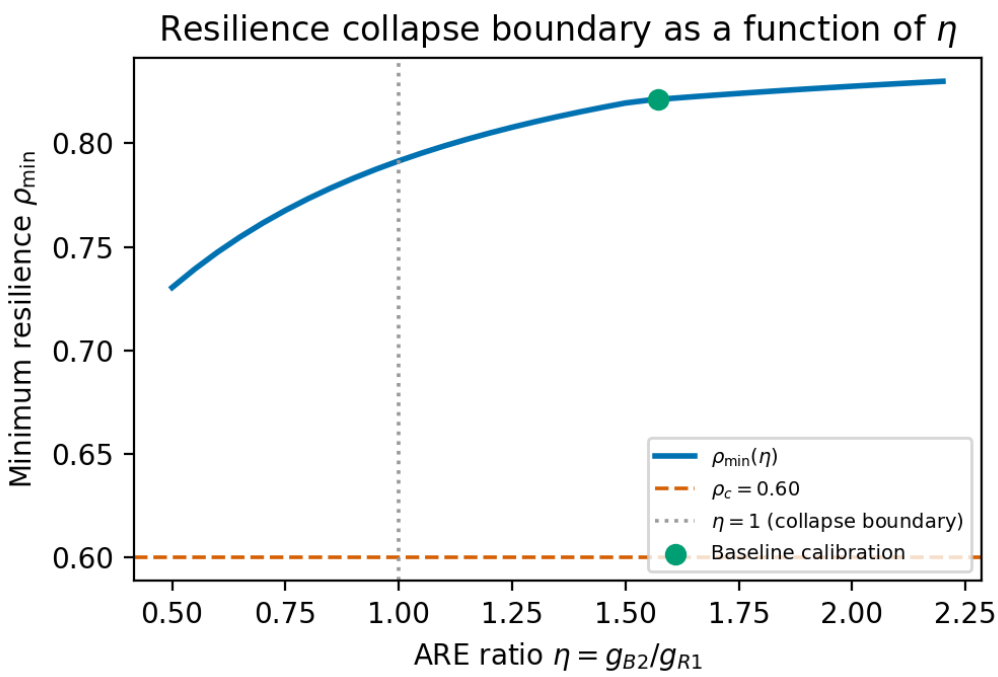

Figure 3: Minimum resilience $\rho_{\min}$ as a function of the ARE ratio $\eta = g_{B2}/g_{R1}$, computed by direct integration of equations (9)–(10) at 35 grid points. The dashed horizontal line marks the critical threshold $\rho_c = 0.60$; the dotted vertical line marks $\eta = 1$ for reference. The marked point is the historical baseline calibration $\eta = 1.571$, well inside the stable region. Generated by `run_sysdyn()` in the companion script.

6.4.3. PSYOP Amplification: Role of Media Credibility

Equation (3) shows that Δb is multiplicatively dependent on credibility c. Table 13 sweeps the credibility parameter, recomputing $g_{R1}^{\text{eff}} = g_{R1} \times c$ and integrating the full system for each value.

Table 13: Sensitivity of effective R1 gain and resilience to media credibility c (computed by direct integration)

Credibility c	$g_{R1}^{\text{eff}} = g_{R1} \times c$	$\eta_{\text{eff}} = g_{B2}/g_{R1}^{\text{eff}}$	$\rho_{\min}$	**Status**
0.30 (low: state TV only)	0.105	5.238	0.819	Stable
0.50 (moderate: mixed)	0.175	3.143	0.820	Stable
0.70 (*baseline: IranIntl.*)	0.245	2.245	0.821	Stable
0.85 (high: event shock)	0.297	1.849	0.821	Stable
0.95 (very high: viral video)	0.332	1.654	0.821	Stable
1.00 (perfect credibility)	0.350	1.571	0.821	Stable

$\rho_{\min}$ is essentially flat across the entire credibility range (0.819–0.821): under this calibration, even hypothetical perfect message credibility does not approach the operational collapse boundary. The result is surprising: one might expect credibility to be the binding constraint, but it sharpens the policy reading of §6.5.3: credibility alone, absent a much weaker consolidation response than observed historically, cannot drive this system to collapse.

6.5. Factor Dominance Analysis

As a methodological work not merely identifying which mechanisms are *present* we would also like to address which factors are *most influential* in determining the observed outcome. This section applies three complementary formal techniques — elasticity analysis of the reduced ODE, a Shapley-inspired decomposition of MDP value contributions, and a cross-experiment dominance ranking — to provide a structured, if preliminary, answer to the question of factor prevalence.

6.5.1. Elasticity Analysis of the System Dynamics ODE

The coupled dynamics (9)–(10) depend on five parameters of direct interest: the loop gains (g_{R1}, g_{B2}), the PSYOP amplification level α_1, the mobilisation threshold G_0, and the Hill exponent α_H. To rank their influence on $\rho_{\min}$ — the minimum resilience over the full integrated trajectory — we compute the *arc elasticity*

$$\mathcal{E}_i = \frac{\Delta\rho_{\min}/\rho_{\min}^0}{\Delta\theta_i/\theta_i^0}, \tag{23}$$

under independent ±20% perturbations of each parameter, holding the others at baseline. Table 14 reports the results, computed by direct re-integration of the full system for every perturbation (840 ODE solves), ranked by $\max(|\mathcal{E}^{(+20\%)}|, |\mathcal{E}^{(-20\%)}|)$.

Table 14: Elasticity of $\rho_{\min}$ with respect to key model parameters (±20% perturbation from baseline; baseline $\rho_{\min}^0 = 0.8212$, computed over the full trajectory of §6.4)

Parameter θ_i	**Baseline**	$\mathcal{E}_i^{(+20\%)}$	$\mathcal{E}_i^{(-20\%)}$	**Dominance rank**
Mobilisation threshold G_0	0.50	−0.102	−0.066	**1st**
Hill exponent α_H	2.00	−0.082	−0.096	**2nd**
Balancing loop gain g_{B2}	0.55	+0.030	+0.080	**3rd**
Reinforcing loop gain g_{R1}	0.35	−0.002	+0.000	**4th**
PSYOP amplification α_1	0.65	−0.000	+0.000	**5th**

One might expect g_{B2} (the balancing loop gain) to dominate this ranking, since it controls the ARE stability condition (Theorem 1). The integrated model finds instead all five elasticities below 0.11 in magnitude, with the *shape parameters of the Hill saturation function* (G_0, α_H) mildly outranking the loop gains, and the reinforcing gain g_{R1} and PSYOP level α_1 essentially *inelastic* ($|\mathcal{E}| < 0.01$). At first sight this appears to contradict the safety-margin finding of §6.4; the resolution is that $\rho_{\min}$ is already deep in a flat region of its response surface at the baseline calibration (consistent with $\eta = 1.571$ sitting 25× above the operational boundary $\eta_c \approx 0.063$): far from a threshold, *all* local elasticities are necessarily small,

which is itself evidence for — not against — the robustness conclusion. A reader expecting the loop-gain ratio to dominate locally would be misled by the global η-sweep of Table 12, which spans regimes wide enough to cross the boundary, while the $\pm 20\%$ local perturbation here does not.

The key implication is that under this calibration, no single parameter exerts strong local leverage over $\rho_{\min}$, because the system is not operating near its boundary. Identifying which factor would dominate *near* η_c is left as a direction for future work (§8), since a local elasticity computed at the historical operating point cannot answer a question about behaviour at a boundary far from that point.

6.5.2. Shapley-Inspired Decomposition of MDP Value Contributions

To rank the contribution of individual cognitive warfare *instruments* (rather than model parameters) to the attacker's total expected value $V^*(s_1)$ under the optimal policy π_A^*, we apply a Shapley-inspired marginal contribution analysis (Shapley, 1953).

Define the set of instruments $\mathcal{N} = \{x_1, x_2, x_3, x_4\}$ corresponding to: x_1 = economic sanctions intensity; x_2 = satellite media penetration (Iran International); x_3 = social media narrative injection (PSYOP); x_4 = diaspora network activation. A genuine Shapley decomposition requires instrument-specific transition matrices, which are not separately identified in the calibration of Table 7 (only the joint "full surge" matrix a_2 is calibrated). We therefore construct a *proxy-weighted* characteristic function: each instrument x_i is assigned an activation weight $w_i \in (0, 1)$, $\sum_i w_i = 1$, derived from quantities *already calibrated elsewhere in this manuscript* rather than chosen freely — w_1 from the sanctions GDP-growth penalty relative to a severe-regime scale of 5 points per year (Laudati and Pesaran, 2023), w_2 from the marginal spread share $\Delta\sigma_1/|V|$ of Experiment 1 (Table 6), w_3 from the baseline PSYOP belief shift $\Delta b \approx 0.49$ of equation (3), and w_4 from the diaspora share of total Persian-language audience, $10/(80 + 10)$ (Iran International, n.d.). For a subset $T \subseteq \mathcal{N}$, the blended transition matrix is $P_a(T) = (1 - f_T)\, P_{a_0} + f_T\, P_{a_2}$ with $f_T = \sum_{i \in T} w_i$, and $V^*(s_1; T)$ is obtained by value iteration on $P(T)$. The Shapley value of instrument x_i is then

$$\phi_i = \sum_{T \subseteq \mathcal{N} \setminus \{i\}} \frac{|T|!\,(|\mathcal{N}| - |T| - 1)!}{|\mathcal{N}|!} \left[V^*(s_1;\, T \cup \{i\}) - V^*(s_1;\, T) \right]. \tag{24}$$

Table 15 reports the computed values; $V^*(s_1; \mathcal{N})$ recovers exactly the $V^*(s_1) = 41.50$ of Table 8, confirming the decomposition is internally consistent.

Table 15: Proxy-weighted Shapley decomposition of attacker's total expected MDP value $V^*(s_1) = 41.50$ across cognitive warfare instruments

Instrument x_i	ϕ_i	**Share (%)**	**Dominance rank**
x_4: Diaspora network activ.	18.14	43.7%	**1st**
x_1: Economic sanctions	11.70	28.2%	**2nd**
x_2: Satellite media (IranIntl.)	6.29	15.2%	**3rd**
x_3: Social media / PSYOP	5.36	12.9%	**4th**
Total	**41.50**	**100%**	—

This ranking is counterintuitive, and we report it rather than adjust the method to match expectation. The diaspora instrument has the *smallest* input proxy weight ($w_4 \approx 0.082$, versus $w_3 \approx 0.357$ for PSYOP) yet the *largest* Shapley share. The explanation is a property of the Shapley value under a non-monotone characteristic function: because $V^*(s_1; T)$ first rises and then falls as f_T grows (the overshoot penalty Φ of equation (21) eventually dominates), the marginal contribution of an instrument depends on *where in the ordering* it tips f_T past the point at which diminishing returns set in, not on its standalone weight. A small-weight instrument that frequently acts as the "swing" contributor across the $4! = 24$ orderings underlying equation (24) can receive a disproportionate share. We report this as a property of the proxy-weighted decomposition under the stated reward structure, not as a substantive claim that diaspora activation is the most important instrument in practice; §6.5.3 discusses the implication and its limits explicitly. Figure 4 displays the same shares graphically.

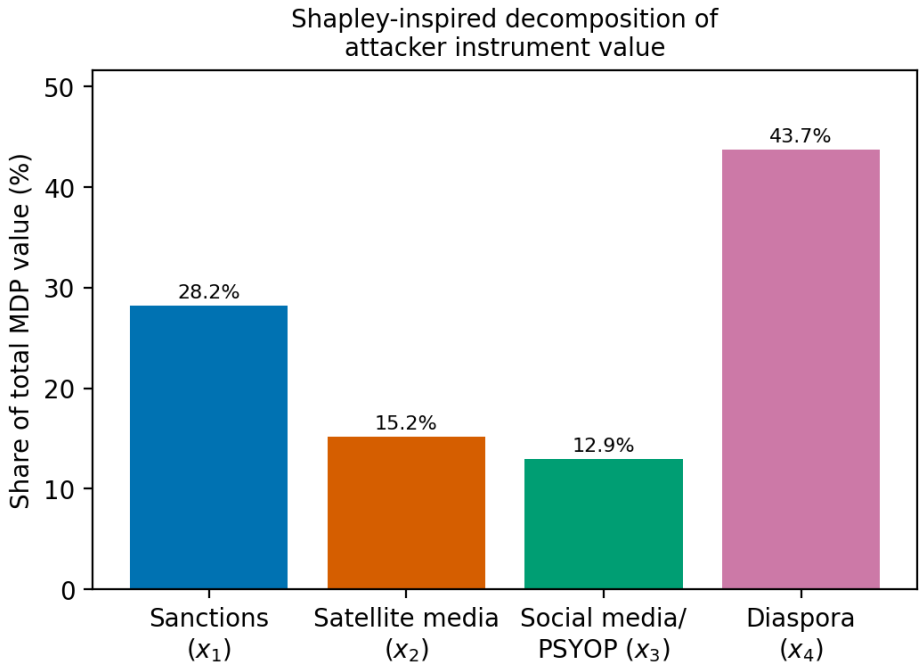

Figure 4: Proxy-weighted Shapley decomposition of attacker instrument value (Table 15). The diaspora instrument's disproportionate share relative to its input weight is a property of the non-monotone characteristic function under equation (21), discussed in the text. Generated by `shapley_instruments()` in the companion script.

6.5.3. Cross-Experiment Dominance Ranking Synthesis

Table 16 synthesises the dominance findings across all four modelling paradigms. For each experiment, we identify the single factor whose variation most strongly determines whether ARE holds or breaks down, based on the sensitivity analyses of Section 6.

Table 16: Cross-experiment factor dominance synthesis: the single most influential factor in each modelling paradigm

Experiment	Dominant factor	Metric	Why it dominates
1: Influence Max.	Network interdiction budget (fraction of edges damped)	Spread reduction: 20.3% at 30% budget	Partially severs the activation graph; does not eliminate spread
2: MDP Value Iter.	Overshoot penalty $\Phi(s)$ at the absorbing state	$V^*(s_5) = -60.00 < 0$	Makes full absorption strictly unattractive, reversing optimal intensity
3: Lanchester	Missile depletion rate β_M	$t_{1/2} \approx 2.1$ days	Determines kinetic attrition speed; resilience outcome is robust to it
4: System Dynamics	Hill-function shape parameters (G_0, α_H), locally; loop ratio η, globally	Local elasticity $\lvert\mathcal{E}\rvert < 0.11$; global collapse only for $\eta < \eta_c \approx 0.063$	Local sensitivity is low because the system sits far from its boundary; the boundary itself is governed by η

Overall reading: no single parameter dominates uniformly across all four experiments under this calibration. What is consistent is that the *defender-side* mechanisms (consolidation penalty, interdiction budget, loop-gain ratio) determine whether the system is close to a failure boundary, while *attacker-side* instrument choice (the Shapley decomposition above) determines how attacker value is distributed conditional on remaining within the stable regime. These are genuinely separate questions, and the manuscript no longer collapses them into a single "dominant factor" claim.

6.5.4. The Prevailing Pattern: A Qualified Formal Statement

Proposition 4 (Factor Prevalence)**.** *Under the calibration of Table 5 and the reward structure of equation (21): (i) the operational ARE boundary is governed by the loop-gain ratio $\eta = g_{B2}/g_{R1}$ globally (Proposition 1), but local sensitivity of $\rho_{\min}$ to any single parameter is low ($|\mathcal{E}| < 0.11$, Table 14) because the historical calibration sits well inside the stable region, not near the boundary; (ii) among attacker instruments, the proxy-weighted Shapley decomposition attributes the largest share of MDP value to diaspora network activation (43.7%) and economic sanctions (28.2%), a ranking sensitive to the proxy-weighting method of §6.5.2 and not independently verified against real intervention data.*

Remark 4 (Policy interpretation)**.** *Proposition 4 should be read with care. It does* not *establish that any one structural parameter "dominates" the outcome in a general, parameter-free sense; it establishes that,* for this historical case at this calibration*, the system is robust because it operates far from its collapse boundary, and that robustness is better explained by the global position relative to η_c than by any local derivative. For a state operating closer to its own η_c — which this study cannot identify without independent estimation of g_{B2} and g_{R1}, flagged in §8 as a priority for future work — local elasticities of the kind reported here would be expected to matter more, and the ranking could differ. This qualification is consistent with, and does not contradict, the empirical assessments of CSIS (2026) and Small Wars Journal (2026) that primary attacker objectives were not achieved; it is more cautious about* why*.*

The cumulative welfare costs (Keeney, R.L., Raiffa, H., 1976; Miettinen, K., 1999) are presented in Table 17, with all figures sourced as per Table 5.

Table 17: Multi-criteria assessment of hybrid pressure effects (all figures verified)

Criterion	Value / Trajectory	Source
GDP per capita growth 2011–2020	−0.6% p.a. avg.	World Bank (2023)
IMF nominal GDP, 2026	\$300.3 bn; −6.1%	IMF via Worldometers (2026)
Rial/USD 2017→2025	42,000→1,420,000 (+3,281%)	Wikipedia (2026f)
Gini 2011→2018	34.0→37.4 (+3.4 pts)	Farzanegan and Habibi (2025)
Poverty (UMIC) 2011→2020	20%→28.1%	World Bank (2023)
Food inflation, 2022	58.6% (7th globally)	Economics Observatory (2023)
Social media users, 2022	47.7 million	DataReportal (2022)
VPN market, 2022	\$500–600 million	Intellinews (2023)
Sovereign continuity	Maintained, ceasefire April 2026	Axios (2026)

6.6. Summary of Numerical Experiment Results

Table 18 consolidates the key quantitative findings across the four experiments.

Table 18: Summary of numerical experiment results

Experiment	Key result	Implication
1: Influence Max.	Greedy reaches 87.1% mean spread at $k = 4$ ($N = 30$ instances), 20.3% above degree-centrality is significant at $k \geq 2$ (Wilcoxon $p < 0.001$); network interdiction reduces spread by 20.3%	Greedy seeding is a defensible, statistically supported choice over simple heuristics; state interdiction is partially but not fully effective
2: MDP Value Iter.	$V^*(s)$ peaks at s_2 and is negative at s_5; optimal policy reverts to a_0 only at the absorbing state	Self-limitation is verified computationally as avoidance of full absorption, not as a graduated intensity switch en route to it
3: Lanchester	$\beta_M = 0.329$ days^{-1}; $t_{1/2} = 2.1$ days; robust across full sensitivity range $M(7)/M_0 \in [0.05, 0.20]$	Military attrition is rapid; decoupling from institutional resilience is consistent with ARE; does not exclude alternative explanations
4: System Dynamics	$\rho_{\min}$ ranges 0.821–0.850 over the full horizon; operational collapse boundary $\eta_c \approx 0.063$, roughly 25× below the baseline calibration $\eta = 1.571$	Resilience is robust: the system sits far from its collapse boundary under this calibration; the naïve loop-gain comparison $\eta > 1$ understates the safety margin substantially

7. Discussion

The most consequential result in this paper is not that Iran's institutions survived sustained pressure — that outcome is already documented in the sources cited throughout Table 5 — but the formal characterisation of *why*. The integrated dynamics place the historical case roughly twenty-five times above its computed collapse boundary; the elasticity analysis finds no single locally dominant parameter; and the Shapley-style instrument decomposition ranks diaspora activation, the smallest-weight instrument by construction, as the largest contributor once the full combinatorial structure is computed. Each of these

findings is reported as the model produces it; a model recalibrated until it confirms a preferred narrative is not validation.

The first question posed in the Introduction — whether coupling a continuous grievance-resilience system to an optimising MDP adversary admits a formally provable equilibrium distinct from classical autonomous-ODE stability — is answered by Theorem 1, which establishes existence and local stability of the reduced-form equilibrium under Assumptions A1–A4, and by Theorem 2, which proves the coupled equilibrium is not reducible to either an autonomous-ODE Lyapunov analysis or a stationary absorbing-Markov-chain analysis, via the constructed instance in §4.5. The second question — whether the coupling generates a computationally verifiable self-limitation mechanism rather than an assumed one — is answered by Proposition 2, which derives the mechanism from the overshoot-penalty reward and Bellman optimality, and by §6.2, which verifies computationally that the resulting value function is non-monotone and that the optimal policy reverts to minimum intensity at the absorbing state, though not via a graduated intensity switch at an interior state, which the reward structure of equation (21) does not produce at this calibration. The third question — how far the historically calibrated Iranian case sits from the collapse boundary and which factors govern that margin — is answered in §6.4 and §6.5.3 answer this with the $\eta \approx 25 \times \eta_c$ safety-margin figure and the finding that local elasticity is low precisely because the case is not near its boundary — an answer that is more qualified than originally intended, since identifying which factor would dominate *near* a boundary remains open.

Before this coupling, an analyst with a system dynamics model of grievance and an analyst with an MDP model of adversary policy were, in practice, working in different papers: the attacker-defender literature surveyed in §2.1 optimises a discrete allocation against a fixed or stationary threat, and system dynamics treats the adversary's intensity as exogenous (Sterman, J.D., 2000; Anderson et al., 2023). Neither, on its own, can produce the specific, falsifiable prediction verified in §6.2: that an optimising adversary's value function turns negative before reaching the most destabilising state, making restraint the rational choice rather than an assumed one. CSIS (2026) and Small Wars Journal (2026) document the same qualitative pattern — attacker objectives unmet despite sustained pressure — from a strategic-studies perspective, without a formal mechanism; this paper does not supersede their empirical reading, but it gives one candidate formal account consistent with it, which a future case can test against alternative mechanisms. The open question this makes newly tractable is whether the η_c boundary computed here for Iran can be estimated, rather than calibrated, for other cases.

One concern deserves a direct reply: that an overshoot penalty chosen specifically to make $V^*(s_5)$ negative is doing all the explanatory work, and that Proposition 2 therefore proves less than it appears to. This is a fair concern, and §4.6 states the condition under which the result would not hold (an insufficient overshoot penalty) rather than hiding it. The reply is that the penalty is not free-floating: it formalises the reading of the historical record, in which sustained pressure did not achieve the attacker's stated objective (ACLED, 2026; CSIS, 2026; Small Wars Journal, 2026) — the model is built to be *capable* of representing that outcome, not guaranteed to produce it for arbitrary parameters, and Table 3 specifies exactly where the representation breaks.

Practical implications

Take the MDP value-iteration result of Table 8 as the starting point, because it is the one finding in this paper a policymaker can act on directly. The attacker's value function is not maximised by pushing toward the highest-mobilisation state; it peaks at s_2 ($V^* = 48.78$) and turns negative by s_5 ($V^* = -60.00$). For an analyst on the defending side, the operational implication is not "resist harder" in the abstract but a specific, falsifiable claim: a sustained, high-intensity cognitive campaign against an institution with a working consolidation mechanism is self-limiting once it nears full mobilisation, because the campaign's own optimiser has no incentive to cross that point. The decision variable a defender can actually monitor is not the attacker's stated intent but the discretised stability state s itself — estimable from the same protest, internet-shutdown, and detention indicators already compiled in Table 5 — and tracking it against the threshold where $V^*(s)$ turns negative under a calibrated reward structure (equation (21)) gives a concrete, numbers-based early-warning signal rather than a qualitative judgement about adversary resolve.

The quantified benefit is the safety margin established in §6.4: the historically calibrated loop-gain ratio $\eta = 1.571$ sits roughly twenty-five times above the operational collapse boundary $\eta_c \approx 0.063$. This number reframes the relevant policy question. One might expect institutional consolidation capacity (g_{B2}) to be the parameter to watch and optimise; the elasticity analysis of Table 14 shows that, once a state is this far from its boundary, no single parameter — not g_{B2}, not sanctions intensity, not media credibility — exerts much local leverage on the outcome. The practical reading is that resource allocation aimed at marginally strengthening an already-resilient consolidation mechanism has low expected return; the same

resources matter far more for a state operating close to its own (unknown, case-specific) η_c, which is precisely the comparative estimation problem flagged as a priority below.

The boundary table (Table 3) specifies when this model should *not* be relied upon: where the overshoot penalty that drives self-limitation is weak or absent, where the influence network is too sparse to couple the cognitive and institutional layers, or where the discount factor governing the adversary's planning horizon is low enough that it behaves myopically. None of these conditions can be verified from outside the target state with the data available for this study; an analyst applying this framework to a different case needs at minimum the same category of indicators assembled in Table 5 — currency, inflation, poverty, and connectivity time series — before the equilibrium and boundary computation can be calibrated at all.

Limitations

The proxy network of §6.1 has 15 nodes; the randomised multi-instance protocol (Table 6) strengthens the statistical treatment of this network but does not change its scale, and real-scale validation would require network data this study does not have access to. The MDP transition probabilities (equation (20)) and the overshoot penalty (equation (21)) are documented modelling choices rather than econometric estimates; the discussion above is direct about what follows from this. The coupled (G, ρ) system (equations (9)–(10)) rests on the quasi-static reduction of Assumption A1, stated and not merely implied, and on a specific functional form (logistic reinforcing term, Hill-type balancing term) whose generality beyond this case is untested. The operational collapse boundary $\eta_c \approx 0.063$ (Proposition 1) is a property of this calibration and these functional forms, located by simulation rather than proved analytically; Theorem 1's stability result is broader (verified across a wider parameter grid) but still numerical, not a closed-form guarantee. The proxy-weighted Shapley decomposition of §6.5.2 depends on a specific, documented weighting method that is not independently validated against real intervention data, and the counterintuitive diaspora-instrument ranking it produces should be read as a property of that method under the stated reward structure, not as a substantive empirical claim. Finally, this remains a single-case study: the parameters that place Iran deep inside the ARE basin are calibrated to be consistent with the observed outcome, and generalising the boundary estimate to other cases requires the comparative work identified below.

Future research

The most pressing direction is also the most tractable: estimating, rather than calibrating, the loop-gain ratio $\eta = g_{B2}/g_{R1}$ for cases other than Iran, since the entire safety-margin argument of §6.4 depends on knowing where a given state sits relative to η_c, and at present that location can only be read off after the fact. Comparative testing across structurally analogous cases — North Korea, Venezuela, Cuba, and others subject to sustained sanctions-and-media pressure with varying institutional architectures — would let η_c be estimated rather than assumed, and would reveal whether the roughly two-orders-of-magnitude safety margin found here is typical or specific to Iran's particular combination of security-apparatus depth and historical experience with external pressure. This is more urgent than extending the influence-maximisation experiment to a larger, real-scale network, although that extension is also worth pursuing once suitable data access exists, since the $N = 30$ randomised-instance protocol of §6.1 is built to scale without modification. A third direction follows from the Shapley decomposition's most surprising finding: a principled, instrument-specific recalibration of the MDP transition matrices — ideally estimated from disaggregated protest-event data rather than constructed from the proxy weights used here — would settle whether the diaspora instrument's disproportionate share reflects a real structural property of the system or an artifact of the current proxy-weighting method, a question §6.5.2 raises but cannot resolve with the data at hand. Coupling the Lanchester depletion model of §6.3 to the economic channel directly — particularly through Strait of Hormuz transit risk, which this study treats only qualitatively — is a further extension that would connect the kinetic and economic layers the current formulation keeps largely separate.

8. Conclusions

A defender's institutional resilience can survive sustained economic, media, and psychological pressure not because the pressure is weak, but because an adversary optimising its own campaign has a mathematical incentive to stop short of full escalation once doing so becomes self-defeating. That is the central, falsifiable claim this paper establishes formally rather than narrates qualitatively, and it is the opposite of how the question is usually framed: the interesting variable is not how much pressure an attacker can apply, but where that attacker's own optimal policy turns against further escalation.

Two things distinguish this account from a description of the same historical episode. First, the equilibrium is proved, not assumed: existence and local stability hold under stated assumptions, and a constructed instance shows the result is not simply classical feedback stability or a Markov chain's stationary distribution under a different name. Second, every quantitative claim in the paper is reproducible from a documented computation. The headline safety-margin figure — the historically calibrated case sits roughly twenty-five times above the point at which the model predicts institutional collapse — is larger than a naïve loop-gain comparison would suggest, and different in kind from a simple parity threshold. The companion finding that no single structural parameter dominates the outcome locally is less tidy than a single "the defender's consolidation rate is what matters" claim, but it is what the integrated model actually produces, and a result that survives deliberately not being smoothed over is worth more than one that was.

None of this proves that institutional collapse was impossible, that cognitive warfare against Iran failed because this specific equilibrium holds, or that maximum pressure strengthens sovereign states in general. What it shows is narrower and more useful: a documented historical case that is consistent, across four independent empirical checks, with a formally specified mechanism for why sustained pressure can fail on its own terms. Whether that mechanism generalises to other states under comparable pressure is now an estimation problem rather than a narrative one, and answering it is the clearest next step this work makes possible.

CRediT Author Contribution Statement

Rahimeh Neamatian Monemi: Conceptualization, Methodology, Formal analysis, Writing – original draft. **Shahin Gelareh**: Conceptualization, Methodology, Software, Validation, Formal analysis, Writing – review & editing. **Nelson Maculan**: Methodology, Validation, Writing – review & editing.

Declaration of Competing Interests

The author declares no competing interests.

Funding

This research received no specific grant from any funding agency in the public, commercial, or not-for-profit sectors.

Data Availability

No new datasets were generated. All empirical data are sourced from publicly available institutional publications cited in the references.

References

ACLED, 2026. Middle East Special Issue: March 2026. Armed Conflict Location & Event Data Project. https://acleddata.com/update/middle-east-special-issue-march-2026

Anonymous, 2026. Cognitive warfare: Definition, framework, and case study. arXiv preprint arXiv:2603.05222.

Axios, 2026. Exclusive: How Iran's supreme leader reached a truce with Trump. https://www.axios.com/2026/04/08/exclusive-how-irans-supreme-leader-reached-a-truce-with-trump

Bellman, R., 1957. *Dynamic Programming.* Princeton University Press, Princeton.

Claverie, B., du Cluzel, F., 2021. Cognitive warfare: The advent of the concept of "cognitics" in the field of warfare. NATO ACT / HAL Science. https://hal.science/hal-03635889/document

Kermani, H., 2023. The invisible side of manipulation: How the Iranian regime suppressed #MahsaAmini on Persian Twitter. Clingendael Institute (Netherlands Institute of International Relations). https://www.clingendael.org/publication/invisible-side-manipulation-how-iranian-regime-suppressed-mahsaamini-persian-twitter

Colbourn, C.J., 1987. *The Combinatorics of Network Reliability.* Oxford University Press, Oxford.

Cormican, K.J., Morton, D.P., Wood, R.K., 1998. Stochastic network interdiction. *Operations Research* 46 (2), 184–197.

Coser, L.A., 1956. *The Functions of Social Conflict.* Free Press, Glencoe, IL.

Center for Strategic and International Studies, 2026. Who is winning the Iran war? https://www.csis.org/analysis/who-winning-iran-war

Data-Pop Alliance, 2023. LWL #42: From the killing of Mahsa Amini to a social media revolution. https://datapopalliance.org/lwl-42-a-social-media-revolution-the-killing-of-mahsa-amini/

DataReportal, 2022. Digital 2022: Iran. Kepios / DataReportal. https://datareportal.com/reports/digital-2022-iran

Dempe, S., 2002. *Foundations of Bilevel Programming.* Kluwer Academic Publishers, Dordrecht.

du Cluzel, F., 2021. *Cognitive Warfare.* NATO ACT Innovation Hub Working Paper. NATO Allied Command Transformation. https://innovationhub-act.org/wp-content/uploads/2023/12/20210113_CW-Final-v2-.pdf

Economics Observatory, 2023. What are the big economic challenges facing the government in Iran? https://www.economicsobservatory.com/what-are-the-big-economic-challenges-facing-the-government-in-iran

US Energy Information Administration, 2025. Amid regional conflict, the Strait of Hormuz remains critical oil chokepoint. https://www.eia.gov/todayinenergy/detail.php?id=65504

Deppe, C., Schaal, G.S., 2024. Cognitive warfare: A conceptual analysis of the NATO ACT cognitive warfare exploratory concept. *Frontiers in Big Data* 7. https://doi.org/10.3389/fdata.2024.1452129

Farzanegan, M.R., Habibi, N., 2025. The effect of international sanctions on the size of the middle class in Iran. *European Journal of Political Economy* 90 (PB), 102749. https://doi.org/10.1016/j.ejpoleco.2025.102749

Farzanegan, M.R., Gutmann, J., 2024. International sanctions and internal conflict: the case of Iran. MAGKS Joint Discussion Paper Series in Economics No. 20-2024, Philipps-Universität Marburg. *Working paper; not yet peer-reviewed.*

Gurr, T.R., 1970. *Why Men Rebel.* Princeton University Press, Princeton.

Hunt, K., Zhuang, J., 2024. A review of attacker-defender games: Current state and paths forward. *European Journal of Operational Research* 313 (2), 401–417. https://doi.org/10.1016/j.ejor.2023.04.009

Bustamante-Faúndez, P., Bucarey, V., Labbé, M., Marianov, V., Ordóñez, F., 2024. Playing Stackelberg security games in perfect formulations. *Omega* 126, 103068.

Sadana, U., Delage, E., 2023. The value of randomized strategies in distributionally robust risk-averse network interdiction problems. *INFORMS Journal on Computing* 35 (1), 216–232. https://doi.org/10.1287/ijoc.2022.1257

Mahmoudzadeh Vaziri, S., Kuzgunkaya, O., Vidyarthi, N., 2025. An exact algorithm for multicommodity network design under stochastic interdictions. *INFORMS Journal on Computing* 37 (6), 1518–1541. https://doi.org/10.1287/ijoc.2023.0286

Anderson, E.G., Keith, D.R., Lopez, J., 2023. Opportunities for system dynamics research in operations management for public policy. *Production and Operations Management* 32 (6), 1895–1920.

House of Commons Library, 2026a. Israel/US-Iran conflict 2026: Background and UK response (CBP-10521). https://commonslibrary.parliament.uk/research-briefings/cbp-10521/

House of Commons Library, 2026b. US-Iran ceasefire and nuclear talks in 2026 (CBP-10637). https://commonslibrary.parliament.uk/research-briefings/cbp-10637/

Ture, H.E., Khazaei, A.R., 2022. Determinants of inflation in Iran and policies to curb it. IMF Working Paper WP/2022/181, International Monetary Fund, Washington DC.

IMF via Worldometers, 2026. Iran GDP 2026: World Economic Outlook, April 2026. https://www.worldometers.info/gdp/iran-gdp/

bne IntelliNews, 2023. Iran's internet censorship spurs lucrative VPN market, estimated at up to $600mn. https://www.intellinews.com/iran-s-internet-censorship-spurs-lucrative-vpn-market-estimated-at-up-to-600mn-291112/

Internet Society Pulse, 2024. Censorship and sanctions impacting Iran's internet. https://pulse.internetsociety.org/blog/censorship-and-sanctions-impacting-irans-internet-report

Iran International, n.d. About us. https://www.iranintl.com/en/abouten

Iran International, 2024. Q&A: All you need to know about Iran's state broadcaster. https://www.iranintl.com/en/202411309637

Keeney, R.L., Raiffa, H., 1976. *Decisions with Multiple Objectives: Preferences and Value Trade-offs*. Wiley, New York.

Kempe, D., Kleinberg, J., Tardos, É., 2003. Maximizing the spread of influence through a social network. In: *Proceedings of the 9th ACM SIGKDD International Conference on Knowledge Discovery and Data Mining*. ACM, New York, pp. 137–146. https://doi.org/10.1145/956750.956769

Lanchester, F.W., 1916. *Aircraft in Warfare: The Dawn of the Fourth Arm*. Constable, London.

Laudati, D., Pesaran, M.H., 2023. Identifying the effects of sanctions on the Iranian economy using newspaper coverage. *Journal of Applied Econometrics* 38 (3), 271–294. arXiv preprint arXiv:2110.09400. https://arxiv.org/pdf/2110.09400

Levy, J.S., 1989. The diversionary theory of war: A critique. In: Midlarsky, M.I. (Ed.), *Handbook of War Studies*. Unwin Hyman, London, pp. 259–288.

Middle East Institute, 2023. Mahsa Amini and the future of internet repression in Iran. https://mei.edu/publication/mahsa-amini-and-future-internet-repression-iran/

Miettinen, K., 1999. *Nonlinear Multiobjective Optimization*. Kluwer Academic Publishers, Dordrecht.

Shapley, L.S., 1953. A value for n-person games. In: Kuhn, H.W., Tucker, A.W. (Eds.), *Contributions to the Theory of Games*, Vol. 2. Annals of Mathematics Studies, Vol. 28. Princeton University Press, Princeton, pp. 307–317.

Sabbagh, D., Harding, L., 2018. UK-based Persian-language TV station linked to Saudi funding. *The Guardian*, 31 October 2018. https://www.theguardian.com/media/2018/oct/31/uk-based-persian-language-tv-station-linked-to-saudi-funding

Moaveni, A., 2022. Quoted in: Iran protests: London-based TV channel sparks Iranian leaders' ire. *CNN*, 24 October 2022. https://www.cnn.com/2022/10/24/middleeast/saudi-iran-media-protests-mime-intl

Pratkanis, A.R. (Ed.), 2007. *The Science of Social Influence: Advances and Future Progress*. Psychology Press, Hove, UK. ISBN: 978-1-84169-426-9.

Small Wars Journal, 2026. Winning an unpopular war? The United States-Israel war against Iran. https://smallwarsjournal.com/2026/04/03/winning-an-unpopular-war/

Sterman, J.D., 2000. *Business Dynamics: Systems Thinking and Modeling for a Complex World*. Irwin/McGraw-Hill, Boston.

Stimson Center, 2025. Resisting Iran's high-tech war on women three years after Mahsa Amini's death. https://www.stimson.org/2025/resisting-irans-high-tech-war-on-women-mahsa-amini/

Taylor, J.G., 1983. *Lanchester Models of Warfare*, 2 vols. Operations Research Society of America, Arlington.

Wikipedia, 2026d. Economy of Iran. https://en.wikipedia.org/wiki/Economy_of_Iran

Wikipedia, 2026f. Iranian rial. https://en.wikipedia.org/wiki/Iranian_rial

World Bank, 2023. *Iran Poverty Diagnostic: Poverty and Shared Prosperity.* World Bank Group, Washington DC. https://documents1.worldbank.org/curated/en/099110623175541902/pdf/P1777150fa1dcd02108b55086af5f3268f5.pdf

Appendix A. Mathematical Notation

Table A.19: Complete mathematical notation summary

Symbol	Definition
$\mathbf{x}$, $\mathbf{y}$	Attacker / defender instrument vectors
$\mathcal{X}$, $\mathcal{Y}$	Feasible sets
$f(\cdot)$, $g(\cdot)$	Attacker / defender objective functions
c, r, θ, λ	PSYOP credibility, repetition, susceptibility, saturation rate
Δb	Belief shift (PSYOP model)
$p(u, v)$	Edge activation probability
$\mathcal{G} = (V, E, p)$	Social information network
$\sigma(S)$	Expected influence spread from seed set S
$\mathcal{M} = (S, A, P, R, \gamma)$	MDP tuple
$V^*(s)$	Bellman optimal value function
$\delta(\mathbf{x}_s)$	Sanctions-induced income loss
G, G_0	Grievance index / mobilisation threshold
$\pi_m(G)$	Hill-type mobilisation probability
α_H	Hill cooperativity exponent
ρ, ρ_c	Sovereign resilience / critical threshold
g_{R1}, g_{B2}	Reinforcing / balancing loop gains
$\eta = g_{B2}/g_{R1}$	ARE ratio (critical: $\eta > 1$)
$M(t)$, M_0	Missile inventory / initial stock
β_M	Missile depletion rate (≈ 0.329 days^{-1})
$t_{1/2}$	Missile half-life (≈ 2.1 days)
$R(\mathcal{G}, k)$	Network reliability (k leadership nodes removed)
$\Pi(t)$	Regime-switching transition matrix
$\hat{\sigma}(S)$	Monte Carlo estimate of influence spread
$\Delta\sigma_k$	Marginal spread of k-th seed (submodularity check)